An Estimate of Tidal Energy Lost to Turbulence at the Hawaiian Ridge

JODY M. KLYMAK

Scripps Institution of Oceanography, La Jolla, California

JAMES N. MOUM AND JONATHAN D. NASH

College of Oceanic and Atmospheric Sciences, Oregon State University, Corvallis, Oregon

ERIC KUNZE, JAMES B. GIRTON, GLENN S. CARTER, CRAIG M. LEE, THOMAS B. SANFORD, AND MICHAEL C. GREGG

Applied Physics Laboratory, and School of Oceanography, University of Washington, Seattle, Washington

(Manuscript received 28 April 2004, in final form 6 September 2005)

ABSTRACT

An integrated analysis of turbulence observations from four unique instrument platforms obtained over the Hawaiian Ridge leads to an assessment of the vertical, cross-ridge, and along-ridge structure of turbulence dissipation rate and diffusivity. The diffusivity near the seafloor was, on average, 15 times that in the midwater column. At 1000-m depth, the diffusivity atop the ridge was 30 times that 10 km off the ridge, decreasing to background oceanic values by 60 km. A weak (factor of 2) spring–neap variation in dissipation was observed. The observations also suggest a kinematic relationship between the energy in the semidiurnal internal tide (E) and the depth-integrated dissipation (D), such that $D \sim E^{1\pm0.5}$ at sites along the ridge. This kinematic relationship is supported by combining a simple knife-edge model to estimate internal tide generation, with wave–wave interaction time scales to estimate dissipation. The along-ridge kinematic relationship and the observed vertical and cross-ridge structures are used to extrapolate the relatively sparse observations along the length of the ridge, giving an estimate of 3 ± 1.5 GW of tidal energy lost to turbulence dissipation within 60 km of the ridge. This is roughly 15% of the energy estimated to be lost from the barotropic tide.

1. Introduction

One of the more perplexing problems in oceanography is the dichotomy between the rate of vertical mixing inferred from the strength of the meridional overturning circulation and the rate directly measured by turbulence profilers. Large-scale properties indicate a diffusivity of $K = 10^{-4}$ m^2 s^{-1} (Munk 1966; Munk and Wunsch 1998; Ganachaud and Wunsch 2000), a number often used in global circulation models. Measurements from microstructure profilers in the open-ocean thermocline indicate that the value is an order of magnitude lower than this, $K = 10^{-5}$ m^2 s^{-1} (Gregg 1989), a number corroborated by dye-release studies (Ledwell et al. 1993). Measurements in the deep ocean are sparse but away from topography seem to have similarly low diffusivities (Polzin et al. 1997). One possible way to provide the mixing that drives the overturning circulation is to find exceptionally high mixing near ocean boundaries. High mixing is found near seamounts (Kunze and Toole 1997), submarine ridges (Althaus et al. 2003), and submarine canyons (Polzin et al. 1996; Carter and Gregg 2002); over deep rough topography (Polzin et al. 1997; St. Laurent et al. 2001); and on continental slopes (Moum et al. 2002; Nash et al. 2004). However, these high mixing measurements are not elevated more than a few tens of kilometers from the topography and do not lead to large basin-averaged diffusivities at depths where there is a large area of open water (Kunze and Toole 1997).

Another closely related question is that of where tidal energy gets removed from the ocean. Oceanic tides put energy into the ocean at a rate of 3.5 TW

Corresponding author address: J. Klymak, Scripps Institution of Oceanography, 9500 Gilman Dr., Box 0213, La Jolla, CA 92093-0213.
E-mail: jklymak@ucsd.edu

(Munk and Wunsch 1998). Much of this is believed to be dissipated in marginal seas because of bottom friction. In the open ocean, bottom friction is much weaker, and energy is believed to be mostly removed by the generation of internal tides (St. Laurent and Garrett 2002). These internal waves eventually dissipate by a number of poorly quantified mechanisms: they can lose energy directly to bottom friction, they can break on other topography (Nash et al. 2004), or they can interact with other internal waves and thereafter cascade to turbulence (Pomphrey et al. 1980; Olbers 1983; MacKinnon and Winters 2005, unpublished manuscript, hereinafter MKW).

The Hawaii Ocean Mixing Experiment (HOME) was designed to examine the energy budget of an important open-ocean site of internal tide generation. The experiment was situated at the Hawaiian Ridge because it is very long (2500 km) and is approximately perpendicular to the barotropic tidal wave, and thus was expected to be efficient at producing internal tides. Inverse calculations on satellite altimeter data indicate that 18 ± 6 GW of energy is removed from the M_2 barotropic tide near the ridge (Egbert and Ray 2000). Recent numerical work estimates that 10 GW radiates away from the ridge as an M_2 internal tide (Merrifield and Holloway 2002, hereinafter MH02). Of the 10 GW, 6 GW radiate away in the first vertical mode, in agreement with inverse calculations of the internal tide made using satellite altimetry (Ray and Cartwright 2001).

In this paper we attempt to quantify the dissipation rate of turbulent kinetic energy near the generation site of the internal tide. Energy not radiated from the ridge as internal tides must be dissipated locally. If the altimetry and modeling cited above are accurate, then there is 8 GW of unaccounted energy that may be fed into local turbulence. Velocities from numerical models indicate that bottom friction is not likely to be an important sink of energy (MH02), so a likely route for this energy is that the internal tide cascades from intermediary internal waves until they reach a scale small enough that they dissipate in the interior of the water column (Henyey et al. 1986). We assume that the turbulence observed in HOME is a direct result of this cascade process and attempt to assess its contribution to the energetics of the cascade. Characterizing turbulence in any environment is challenging because of the intermittency of the phenomena that cause it. It is made more daunting when attempting to do so over as large an area as the Hawaiian Ridge. The ridge is 2500 km long with topography that varies from islands that protrude above the water to wide 4000-m-deep channels. There is also the added variability of the tidal forcing, which undergoes a daily modulation by the diurnal tides and a fortnightly modulation by the S_2 tide.

We quantify the turbulence using four instruments deployed during two field seasons (2000 and 2002): two loosely tethered shallow-water profilers able to profile to 1000-m depth, a free-falling profiler able to profile to 4000-m depth, and a horizontally towed vehicle (section 2). We characterize the dissipation observed by these instruments, detailing the depth, and along-, and across-ridge variability (section 3). These observations combine to give a two-dimensional estimate of the dissipation at one of the prominent generation regions (section 4). We then present how the dissipation varies with the generated internal tide, both in the fortnightly cycle and along the 2500 km of the ridge (section 5). Combined, these findings allow us to make a rough total for the local dissipation at the ridge (section 6). We conclude with a short discussion of the implications of our results (section 7).

2. Data collection

a. Instruments

Four instruments are discussed in this paper. The two tethered profilers used were the advanced microstructure profiler (AMP), capable of profiling to 1100-m depth, and Chameleon, which profiles to 1000 m [both instruments are described and compared in detail in Moum et al. (1995)]. These instruments characterized near-surface turbulence near the ridge, particularly in the relatively shallow saddles between islands. They collect the usual conductivity–temperature–depth (CTD) data, in addition to being equipped with shear probes. The shear probes are very sensitive to velocity fluctuations and are routinely used to make estimates of energy dissipated at the smallest scales (Moum et al. 1995). Briefly, a spectrum of the shear signal is computed in finite blocks (usually between 1 and 4 m) and then fit to an empirical spectrum (Wesson and Gregg 1994) that relates the fluctuations to the rate of turbulence dissipation (W kg^{-1} or $m^2 s^{-3}$).

The absolute velocity profiler (AVP) is an untethered vertical profiler that can be deployed to 6000 m (Sanford et al. 1985). In addition to a CTD and shear probes, the AVP was equipped with electromagnetic sensors for estimating water column velocities. These measurements allowed calculation of velocity and vertical displacement perturbations, and hence internal wave energies and fluxes. The towed instrument Marlin measures CTD quantities and turbulence dissipation over long horizontal tows at fixed depths up to 3400 m (Moum et al. 2002).

Both Marlin and AVP collected data at depths where

the open-ocean dissipation rates are beneath the noise levels of the instruments. A noise floor was determined in a slightly different way for each instrument. For AVP, noisy data were removed empirically based on statistics from a quiet portion of each profile [see Lee et al. (2006) for details]. For Marlin, the shear-probe signal was correlated with an accelerometer signal, following Levine and Lueck (1999). The coherent part was removed from the shear signal and the spectra recomputed and fit to the universal spectrum, giving an improved estimate of the dissipation rate. If this procedure lowered the estimate of dissipation by more than 50% the data were deemed to be too contaminated by vibration. For both instruments noisy data were set to $\varepsilon = 10^{-11}$ m^2 s^{-3}. The lognormal distribution of turbulence usually means that the average dissipation rate is dominated by a few events, so, with long enough averaging intervals, mean dissipations below the noise level can be determined with small inaccuracy (Moum et al. 2002). Marlin had a noise level near $\varepsilon = 3 \times 10^{-9}$ m^2 s^{-3} for the 2000 cruise and $\varepsilon = 3 \times 10^{-10}$ m^2 s^{-3} for the 2002 cruise. AVP had a higher noise level due to vibrations and a drop-weight ahead of its nose, so that the noise level was closer to $\varepsilon = 10^{-8}$ m^2 s^{-3}.

In this paper we normalize turbulence dissipation by the mean stratification, removing the $\varepsilon \sim N^2$ dependence observed in the open ocean (Gregg 1989; Polzin et al. 1996). This allows us to compare turbulence dissipation rates at different depths in terms of a turbulent diffusivity of density (m^2 s^{-1}):

$$K_\rho = \Gamma \frac{\varepsilon}{\langle N^2 \rangle}, \tag{1}$$

where $\Gamma = 0.2$ is an empirical mixing efficiency (Osborn 1980; Moum 1996). For the open ocean, $K_\rho \approx 10^{-5}$ (m^2 s^{-1}). The mean stratification $\langle N^2 \rangle$ is calculated from the average of AVP profiles during the field year in 2000 (see below) by differentiating the vertical density profiles ($N^2 = -g\rho^{-1}\partial\rho/\partial z$). The hydrography of the region remained approximately constant over both field years and over the length of the ridge (Fig. 1). For most parts of the water column there are only small differences in N^2, no larger than 20% at any one depth. The most significant difference was found between 500 and 1200 m at French Frigate Shoals and Kauai Channel. These small differences do not affect the results of this paper.

b. Sampling scheme

The Hawaiian Ridge stretches from Midway Island in the west (28°13′N, 177°22′W), to the Island of Hawaii in the east (Fig. 2). The ridge rises from deeper than 4000 m to near the surface in less than 20 km. The barotropic tide passes over the ridge as a tidal wave sweeping to the southwest with barotropic currents approximately perpendicular to the ridge reaching 0.031 m s^{-1} in deep water away from the ridge (Table 1). The energy lost from the barotropic tide is thought to go into dissipation and the internal tide. The internal tidal component has been simulated in a primitive equation model by MH02, who found that internal tide radiation was strongest near French Frigate Shoals and Kauai Channel; for that reason much of HOME focused on these sites.

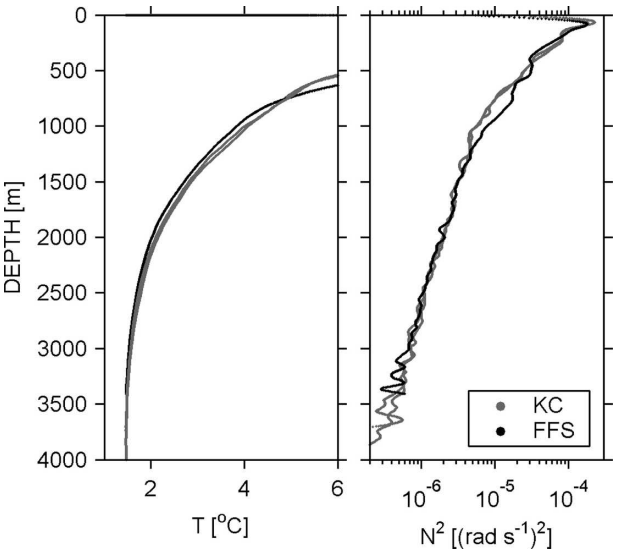

FIG. 1. Cruise-mean profiles at Kauai Channel and French Frigate Shoals, collected from the profiler AVP. There are two traces at Kauai Channel, one for HOME 2000 and the second for HOME 2002. Temperature data are 2-m averages, and buoyancy–frequency data are 2-m data smoothed to 50 m.

Data were collected over two field seasons in 2000 and 2002. There were two AVP cruises. AVP drops were made in October 2000 at 14 stations along the ridge (Fig. 2, black diamonds), nominally at the 3000-m isobath (Lee et al. 2006). Collection was weighted toward locations where numerical modeling (MH02) predicted enhanced internal wave flux (Kauai Channel, French Frigate Shoals, and Nihoa); however, stations were also occupied at regions suspected of weak internal wave flux (i.e., Necker Island). Stations were occupied for approximately 20 h, allowing four to six casts to depths greater than 3000 m. More AVP data were collected in 2002 but will not be discussed in this paper.

Marlin data are presented from two cruises. In 2000, data collection was concentrated at French Frigate Shoals (FFS; Fig. 2b), with cross- and along-ridge tows at depths specified in Table 2. The cross-ridge tows ran through the 700-m-deep saddle point between the two

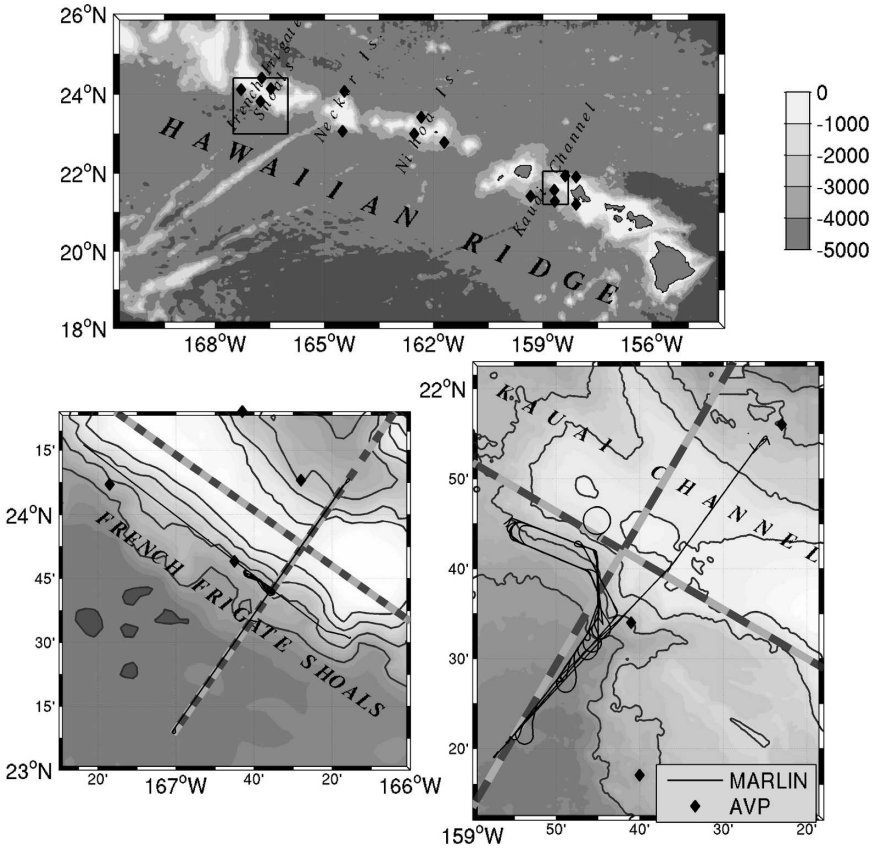

FIG. 2. Data locations in this paper. (top) Plot of the whole ridge, with AVP drops marked as black diamonds. (bottom) Close-ups of (left) French Frigate Shoals and (right) Kauai Channel, with Marlin tows drawn in black. Contour intervals are 1000 m. The axes with alternating gray bands define the along- and cross-ridge coordinate systems at each saddle; shades alternate every 5 km.

shoals. The along-ridge tows ran from shoal to shoal. In 2002 we ran Marlin in Kauai Channel (KC) on a cross-ridge track that passed over the 1000-m contour of Kaena Ridge, off the southwest coast of Oahu (Fig. 2c). This track was aligned along the line of moorings deployed by other HOME investigators. A second mode of deployment was to perform a dog-leg pattern that approached the ridge until the 3000-m isobath, then turned northwest to follow that isobath until the western extent of the 2000-m isobath. A return track was made slightly southwest of this track. This was repeated at four depths (Table 2).

TABLE 1. Tidal constituents in deep water away from the ridge [predicted using tidal constituents described in Egbert and Ray (2000)].

ω	u (m s^{-1})	v (m s^{-1})	$\lvert u\rvert$ (m s^{-1})
S_2	0.006	0.007	0.012
M_2	0.019	0.025	0.031
K_1	0.004	0.006	0.007

Data from two tethered profilers, AMP and Chameleon, are discussed below. Tethered profiler data were concentrated on the highly energetic saddles at KC and FFS.

For the remainder of the paper we will refer to the southwest side of the ridge as the "south" side and the northeast side as the "north" side. Spatial coordinates are relative to the mean ridge direction, with $x > 0$ in the southeast direction and $y > 0$ in the northeast direction. These coordinates are rotated slightly differently at FFS and KC (Fig. 2). When we consider the whole ridge a slightly different angle is used again (section 6).

TABLE 2. Summary of Marlin deployment depths.

Location	Purpose	Depths (m)
FFS	Cross ridge	500, 1000, 1500
	Along ridge	1000, 1500
KC	Cross ridge	700, 900
	Dog leg	700, 1800, 2400, 3000

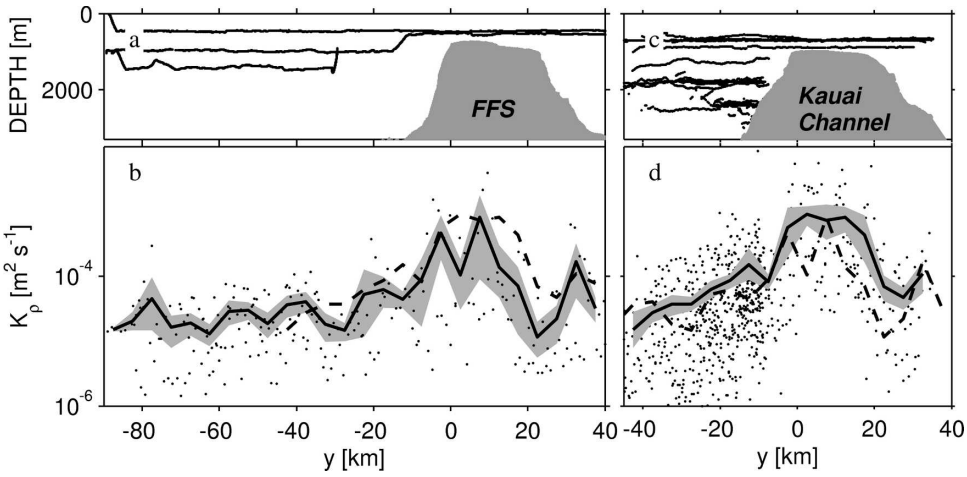

FIG. 3. Turbulence dissipation (normalized by background stratification) in cross-ridge direction for (b) French Frigate Shoals and (d) Kauai Channel. Bootstraps are on 960-s averages (dots) binned in 5-km-wide data bins. Dashed line in (b) is a comparison with the mean line in (d); the dashed line in (d) is the comparison with (b). (a), (c) The Marlin trajectory and the topography of the ridges.

3. Observed structure of dissipation

In this section we characterize the turbulence dissipation over the ridge. The cross-ridge structure of the turbulence was captured by the horizontal Marlin tows. The vertical structure of the dissipation was well resolved on the flanks of the ridge by AVP, and on the saddles between the islands by AMP and Chameleon. The data presented here are also compared with an idealized structure (indicated on the plots with dashed lines), which we will describe in the next section.

a. Cross-ridge structure

The cross-ridge structure of the turbulence was resolved by the Marlin tows across the ridge at FFS and KC. The data at FFS were collected just before peak spring tide, 21–25 November 2000, with two tows at 500-m depth over the ridge, and 500, 1000, and 1500 m south of the ridge (Fig. 3a). The data at KC were collected during spring tide during 20–27 October 2002. There were two repeats at each depth of the dog leg (700, 1800, 2400, and 3000 m), and three repeats over the ridge crest, two at 700- and one at 900-m depth (Fig. 3c).

The structure of the dissipation was similar at the two locations. Highest dissipations occurred directly over the ridge, causing mean diffusivities to reach $K_\rho > 10^{-3}$ m^2 s^{-1}, and individual 5-km averages of $K_\rho \approx 10^{-2}$ m^2 s^{-1}. High diffusivities extend across the width of the saddles, approximately 20 km. As the water deepens, diffusivities fall off quickly, so that $K_\rho \approx 10^{-4}$ m^2 s^{-1} 10 km off the saddle. Diffusivities continue to decrease farther off ridge until they reach the oceanic background of $K_\rho \approx 10^{-5}$ m^2 s^{-1} 40–60 km south of the ridge.

b. Vertical structure—Ridge flanks

AVP drops along the 3000-m isobath allow comparison of the along-ridge variability of the dissipation. Dissipation was stronger at all depths at KC and FFS compared to Nihoa or Necker Island (Fig. 4). Midwater column diffusivities at Nihoa and Necker were little higher compared to the open-ocean value of $K_\rho = 10^{-5}$ m^2 s^{-1}, whereas those at KC and FFS were near $K_\rho = 10^{-4}$ m^2 s^{-1}. All four locations had enhanced diffusivities that started 1500 m above the seafloor and increased to a maximum at the seafloor.

There was considerable variability at any one location, even in the 100-m bin averages (Fig. 5). At any given depth, diffusivities varied by an order of magnitude, and the bootstrap confidence intervals for 23 profiles were at least a factor of 2 on either side of the mean. Variability naturally arises in turbulence datasets but is compounded in this case by the spatial variability of the profiles that went into each location average and by the spring–neap cycle of the tidal forcing.

The consistency between AVP and Marlin observations is quite good at both FFS and KC (Fig. 5, circles and diamonds, respectively). For these comparisons, Marlin data collected in water depths between 2700 and 3300 m were averaged depending on the nominal depth of each tow. The Marlin data from 1400 m above the bottom at KC were higher than the AVP average at KC, but otherwise the general trends of the datasets are

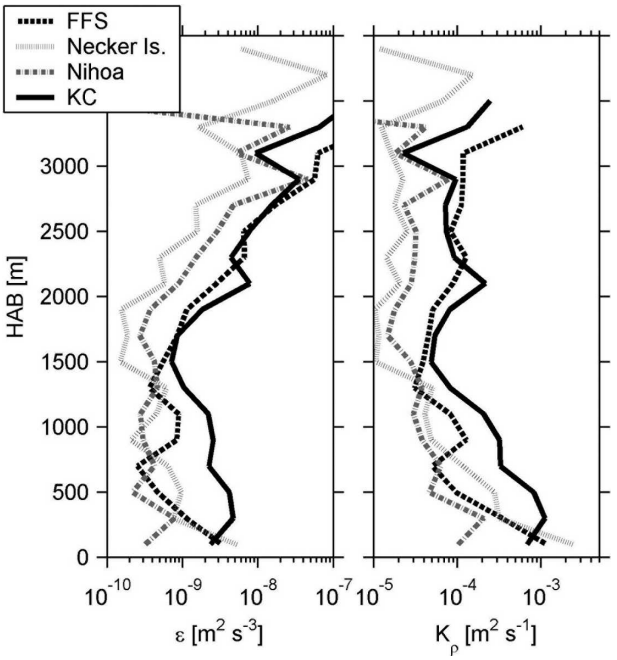

FIG. 4. Location averages of dissipation and diffusivity from AVP data collected at the 3000-m isobath during the HOME 2000 cruise. Data are binned in 200-m averages and plotted as height above bottom (HAB).

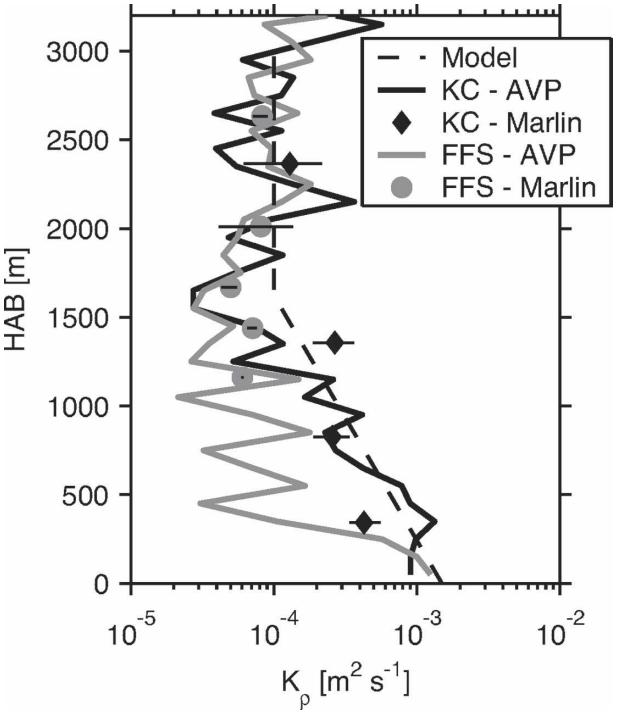

FIG. 5. Vertical structure of diffusivity (dashed) compared with vertical averages from profilers at 3000-m depth on FFS and KC.

the same. At that these mid-depths, where both N^2 and dissipation levels are low, AVP dissipation rates are most likely to be underestimated, and some unevenness appears in the profiles between under- and well-estimated bins. The modeled structure (dashed line, discussed below) is an average between the two measurement types.

c. Vertical structure—Ridge top

The high dissipation observed on top of the ridge by Marlin is very important to the cross-ridge averages (see below), so quantifying the dissipation there is important. Ridge-top data were collected at FFS using the profiler Chameleon, with 58 profiles between 0322 UTC 26 November and 0804 UTC 27 November 2000. The time series of data show coherent patches of turbulence that migrate vertically through the measurement domain (Avicola and Moum 2005, unpublished manuscript). When averaged, the patches yield a diffusivity profile that increases from a minimum of $K_\rho \approx 10^{-4}$ m^2 s^{-1} at the surface to a maximum of $K_\rho \approx 5 \times 10^{-3}$ m^2 s^{-1} at the seafloor (Fig. 6). This profile agrees well with the average Marlin tows at 700-m depth.

More comprehensive measurements were made at KC using the tethered profiler AMP (Fig. 6), covering the eastern side of the ridge in waters shallower than 1100 m. More shallow than deep profiles were collected, so a simple average is inappropriate. Instead, we perform an area-weighted average of all the profiles collected in discrete water depths. Above 500 m, this weighted average is dominated by shallow parts of the ridge where there is heightened dissipation from high-

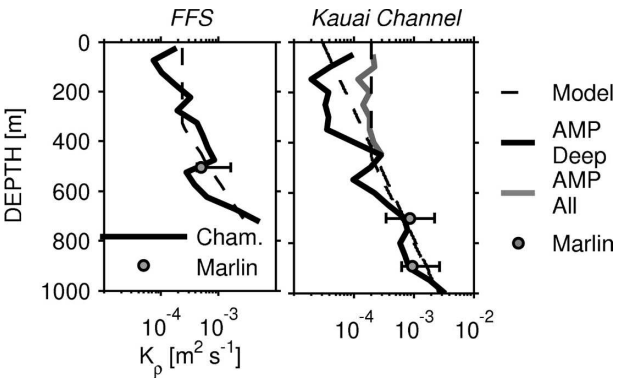

FIG. 6. Ridge-top dissipations. (left) Dissipation profiles at FFS using Chameleon. Data are from a 29-h time series at a single station. The dot is data from the two Marlin tows made over FFS at 700-m depth, averaged between 0 and 20 km (Fig. 3). The dashed line is the model proposed in section 4. (right) Profiles at KC using AMP. Dark line is the average of profiles made in water depths greater than 500 m, light line is the average of all ridge-top data. The dashed lines are two models discussed in section 4.

wavenumber, nonlinear waves formed by the tide passing over rough bathymetry (Carter et al. 2006). If we do not include these waves (Fig. 6, dark line), then the character of the profile is similar to FFS, monotonically increasing toward the seafloor. The high dissipation in shallow water increases the profile above 500 m so that it has a constant value $K_\rho \approx 2 \times 10^{-4}$ m^2 s^{-1}. The Marlin data, averaged on the ridge top between $y = 0$ and $y = 20$ km (Fig. 6, circles), agrees with the AMP data at 700 and 900 m.

4. A structure to describe the cross-ridge dissipation

The data discussed above suggest a common pattern for the dissipation across the ridge, which we use as an aid to integrate the dissipation. We assume the pattern that is separable in depth and cross-ridge direction and expressed as a diapycnal diffusivity [Eq. (1)]:

$$K(y, z) = K_0 \chi(y/L) \zeta(z/H), \tag{2}$$

where H is the total water depth, z is the height above the bottom, $L = 1$ km is an arbitrary horizontal length scale, and $K_0 = 10^{-5}$ m^2 s^{-1} is the open-ocean background diffusivity. We now determine χ and ζ based on the available data.

The vertical dependence, $\zeta(z/H)$, was chosen based on the data in Figs. 5 and 6. We model it as a 15-fold increase of the diffusivity in the bottom 55% of the water column, with the values linearly interpolated in log space:

$$\zeta(z/H) = \begin{cases} 1 & z/H > 0.55 \\ 10^{1.18[1-(z/0.55H)]} & z/H < 0.55 \end{cases}. \tag{3}$$

This function is compared with the profiles at the 3000-m isobath (Fig. 5, dashed line) and profiles atop the ridge (Fig. 6, dashed line). The absolute value of the modeled profiles is set by the y dependence given below and an arbitrary scale factor. The shape of the model agrees well with the profiles at the 3000-m isobath and the AMP measurements at KC. However, it does not follow the Chameleon measurements at FFS or the AMP measurements that excluded the high dissipation in the upper 500 m, so a second ridge-top model with a monotonically decreasing profile is also considered (and shown in Fig. 6).

We chose a cross-ridge structure based on the data presented in Fig. 3, with a slight modification that accounts for the enhanced depth dependence over the ridge (Table 3). Values of $\chi(y/L)$ were interpolated in log space between the values given in Table 3 to give the structure in Fig. 7. This structure gives lower diffusivities than were measured over the ridge top by the 700-m-deep Marlin tows, because, in 1000 m of water, a 700-m-deep tow will have diffusivity enhanced by a factor of 3.1 [Eq. (3)], so χ is reduced by 1/3.1 over the ridge. When the vertical and horizontal structure functions are combined, they give a $K(y, z)$ in agreement with the 700-m-deep tows (Fig. 7).

TABLE 3. Cross-ridge dependence $[\chi(y/L)]$ of diffusivity with $L = 1$ km.

y/L	−60	−10	0	7
$\log_{10}[\chi(y/L)]$	0	1	1.3	1.3

We apply this structure of diffusivity to the section at KC (Fig. 8). Dissipation is inferred from K as $\varepsilon = 5KN^2$. Note that the N^2 dependence tends to deemphasize the deeper dissipation, though there is still a halo of elevated turbulence near the seafloor. The total dissipation in the two-dimensional section can be arrived at by integrating

$$\mathcal{D}(x) = \int_A \rho\varepsilon \, dy \, dz, \tag{4}$$

where the units (W m^{-1}) represent energy lost to turbulence dissipation per unit meter along the ridge. For the KC section in Fig. 8 $\mathcal{D}(x_{\mathrm{KC}}) = 1.6$ kW m^{-1}, where the notation x_{KC} is used to emphasize that this value is only applicable at Kauii Channel. Of this dissipation, 0.7 kW m^{-1} occurs on the flank of the ridge (shallower than 3000 m) and 0.6 kW m^{-1} on the ridge crest (shallower than 1000 m).

A lower estimate for the ridge-crest dissipation is arrived at if we use a model that reflects the Chameleon and AMP profiles in water deeper than 500 m, and therefore away from the nonlinear effects at the edge of KC. We modified the model to have a log-linear increase from the surface to the seafloor so that the dif-

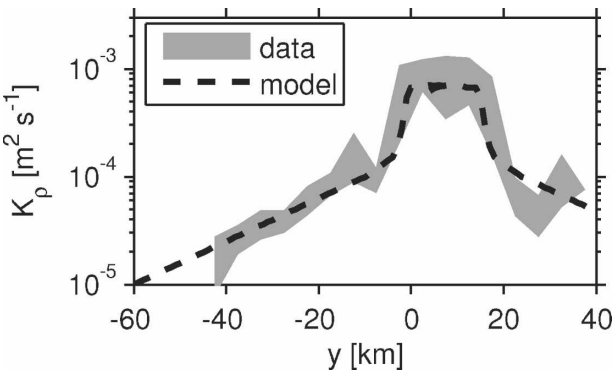

FIG. 7. Horizontal structure function (dashed) compared with data from 700-m depth tows at KC (solid).

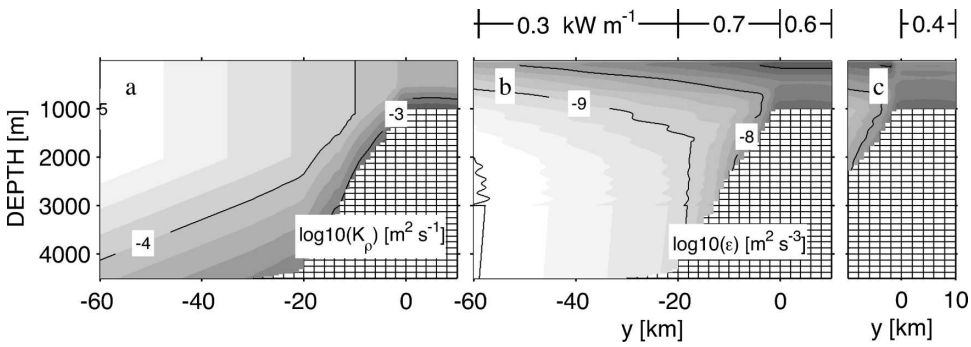

FIG. 8. Two-dimensional structure of (a) the diffusivity and (b) the dissipation inferred from the modeled diffusivity K. The integrated dissipation rates on and off ridge of the 3000-m isobath are shown in (b). (c) The dissipation determined using the weaker dissipation profile at the ridge top (Fig. 6b).

fusivity is 100 times as high at the bottom as at the surface, in rough agreement with the profiles at both FFS and KC (Fig. 6). This gives a 33% lower estimate of the ridge-top dissipation at KC of 0.4 kW m^{-1}, and a total of $\mathcal{D}(x_{\mathrm{KC}}) = 1.4$ kW m^{-1} for the whole section.

5. Relating dissipation to the internal tide

a. Spring–neap tidal variability

We did not resolve the variability of turbulence on a daily time scale with our measurements. No pattern could be seen in the 1-day Chameleon station at FFS. Other work at the ridge indicates that there is dissipation near the seafloor that is phase locked to the barotropic tide (Levine and Boyd 2006), but this was not found aloft. Perhaps daily patterns would be observed after sufficient averages at a single site, but ship time was spent collecting spatial rather than temporal information.

There is evidence of a fortnightly cycle of the dissipation, but it is not strong. The fortnightly variability of the tidal velocity at the ridge is approximately a factor of 2 (Fig. 9a). We use the 15-km stretch of Marlin data from the dog-leg parallel to the ridge as a time series; there was no systematic along-ridge structure found in this part of the dog leg. Mean diffusivities were constant with depth between occupations of the dog leg, except for the shallow tows ($z \approx 700$ m), where there was more variability (Fig. 9b). There was a tendency for the tows made on the leg farther from the ridge (gray symbols) to have weaker diffusivities than tows made on the leg closer to the ridge (black symbols), consistent with the

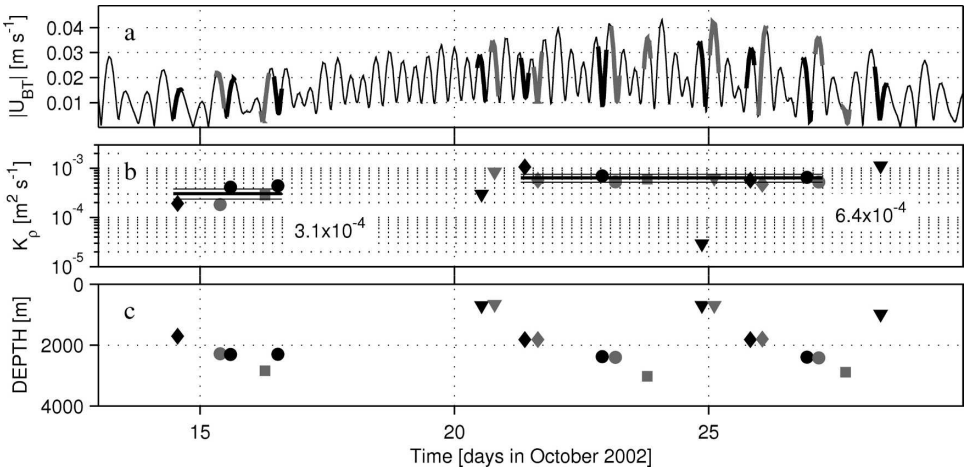

FIG. 9. Spring–neap variation of dissipation near the ridge. (a) Absolute value of the tidal velocity estimates in deep water Kauai Channel [21°12′N , −158°54′W from the barotropic model used by Egbert and Ray (2000)]. (b) Mean diffusivities between -20 km $< x < -5.5$ km in the along-ridge stretch of the dog leg. The symbol shapes correspond to the nominal depth of Marlin as shown in (c), and shading is for the near-ridge half of the section (black) and the off-ridge half (gray). (c) The median depth of the tow.

offshore decay observed above (Fig. 3). Excluding the shallow tows, we compute the mean diffusivities to be $K_\rho \approx 3 \times 10^{-4}\text{m}^2\,\text{s}^{-1}$ for neap and $K_\rho \approx 6.3 \times 10^{-4}\,\text{m}^2\,\text{s}^{-1}$ for spring. Therefore, a factor-of-2 increase in the tidal amplitudes only corresponds to a factor-of-2 increase of the turbulence dissipation.

The weak dependence on the barotropic forcing is somewhat surprising. Simple models of tidal generation, such as the knife-edge model discussed below [first introduced by Stigebrandt (1980)], predict that the production of internal tides, and therefore dissipation, scales quadratically with the barotropic velocity (u_{bt}^2). For the two time periods above, u_{bt}^2 increases by a factor of 3.4 between neap and spring, considerably larger than the observed increase in dissipation. The two estimates can be brought into agreement if we assume that there is a temporal smoothing of the dissipation due to the time it takes for energy to cascade from the internal tide through the broadband internal wave field, and then to turbulence. Smoothing by 5 days reduces the spring–neap variability of u_{bt}^2 to a factor of 2. Five days is a fast time scale for removing energy from the internal tide according to wave–wave time scales cited in Olbers (1983). However, recent modeling indicates that 5 days is not unreasonable when the internal tide is propagating in a coherent direction (MKW). It is possible that analysis of mooring data will reveal a more accurate picture of spring–neap variations.

b. Along-ridge variability

There are large changes in the strength of the dissipation along the ridge at the four locations sampled with the deep profiler AVP (Fig. 4). There was a similar change in the M_2 tidal energy. A reasonable hypothesis is that stronger internal tide generation will produce stronger turbulence dissipation. We test this hypothesis by comparing the integrated dissipation with integrated wave-energy quantities measured by AVP at all 15 stations along the ridge (Fig. 10). The integrated dissipation rate (W m^{-2}) is calculated as

$$D = \left\langle \int \rho\varepsilon \, dz \right\rangle, \tag{5}$$

where the brackets denote averaging over a tidal period. The M_2 baroclinic energy density (J m^{-2}) is calculated as

$$E = \left\langle \frac{1}{2} \int \rho(u'^2 + v'^2 + N^2\zeta^2)\, dz \right\rangle, \tag{6}$$

where u', v', and ζ are perturbation velocities and displacements, fit to an M_2 frequency. Energy fluxes measured with AVP compare well with the numeric model

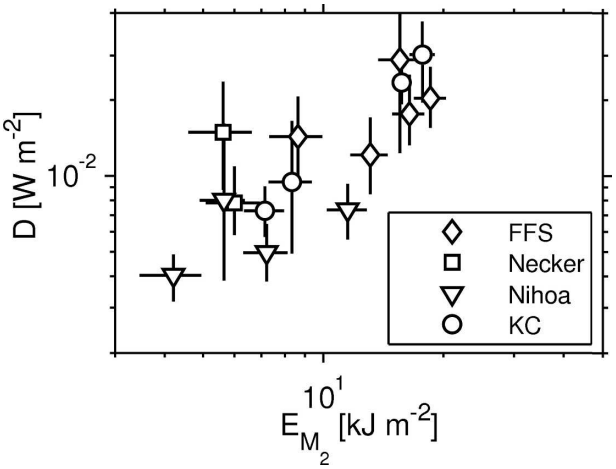

FIG. 10. Relation between depth-integrated M_2 energy density E_{M_2} and depth-integrated dissipation rate D. Error bars on the energy density are calculated by a Monte Carlo analysis, assuming that the tide is superimposed on a broadband internal wave continuum with additional energy near the inertial frequency (Nash et al. 2005; Lee et al. 2006). Error bars in the integrated dissipations are bootstrap estimates on the station averages.

presented by MH02, particularly in the regions of high energy, FFS and KC (Rudnick et al. 2003; Lee et al. 2006). The depth-integrated dissipation, D, is larger where E is larger (Fig. 10).

In what follows below, we attempt to use this relation to extrapolate the dissipation near the Kauai Channel to the rest of the ridge system. To do this, we use the tidal energy density in the Merrifield and Holloway (2002) numerical model. First we ensure that the energy density at the AVP stations and similar locations in the numerical model agree (Fig. 11a). The 4-km grid numerical model estimates have been smoothed horizontally by three grid spaces in each direction, removing granularity in the model. A neutral regression of the two energy estimates indicates good agreement, if the three stations with the weakest energy are excluded from the fit. AVP overestimates the M_2 energy at these stations because the limited number of profiles does not adequately separate the M_2 and broadband internal wave energy unless the M_2 energy is above 5 kJ m^{-2} [see Lee et al. (2006) for a complete discussion]. Attempting to correct for this effective noise level brings these three stations into closer agreement in the model (Fig. 11b).

A power-law fit to the data in Fig. 10 indicates that $D \sim E^{1.2\pm0.2}$ (Fig. 11c). The error of the energy density in log space was, on average, a factor of 2.5 smaller than the error of the dissipation, so it was accorded more weight in the fit. A lower power law is found if we use the same method to fit the dissipation versus the energy density from the numerical model, $D \sim E^{0.5\pm0.15}$

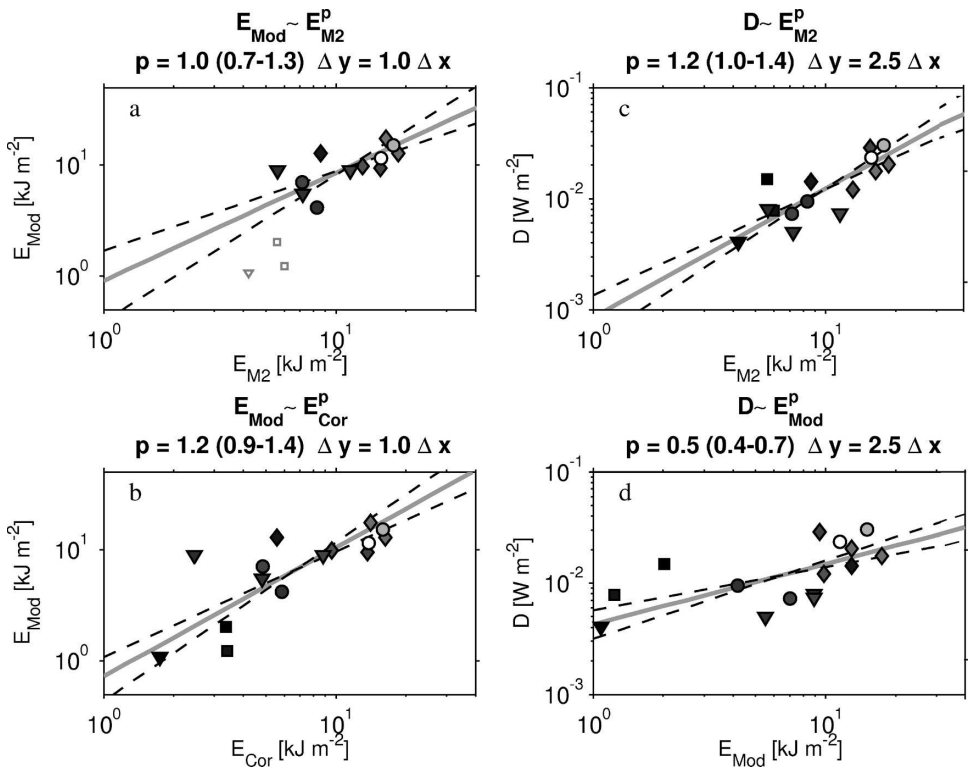

FIG. 11. (a) Energy density measured with AVP vs that predicted by MH02. Stations are shaded proportional to the weight used in the neutral regression. The three grayed-out stations are not used in the fit. The neutral regression (Marsden 1999) is made so that each ordinate is equally weighted. Correlation coefficient is $R^2 = 0.8$. (b) The same data, refit with all stations corrected for the AVP's noise level; $R^2 = 0.8$. (c) Comparison of depth-integrated dissipation and observed energy density (same data as Fig. 10); the regression coefficient is also $R^2 = 0.8$. (d) Comparison of depth-integrated dissipation and energy density from the numerical model; $R^2 = 0.65$.

(Fig. 11d). This is mostly because of the three stations with the weakest energy. If we use the corrected energies (E_{Cor} from Fig. 11b), we get a slightly stronger power law, between the two extremes shown here. Below, we acknowledge that this power law is a major unknown of our analysis and use a spread of between $p = 0.4$ and 1.4 to extend the dissipation estimate along the ridge.

c. *Reconciling the energy density with the dissipation estimates*

The scaling between the energy density and vertical dissipation integration is uncertain from this limited dataset. However, a simple model for the energy cascade supports this scaling and is developed in detail in the appendix. Briefly, if we assume that the tidal radiation can be predicted by a knife-edge model (i.e., St. Laurent et al. 2003; Llewellyn Smith and Young 2003) given a ridge depth, stratification, and barotropic velocity, we can calculate the energy density, E_n, in each vertical mode n (Fig. 12). The energy density depends quadratically on the barotropic velocity and in a complicated manner on the ridge height and stratification. Energy density per mode roughly scales with n^{-2}. The energy flux of each mode is easily calculated from the modal phase speed c_n as $F_n = c_n E_n$.

A simple way to get the observed scaling between dissipation and the energy density is to note that the flux convergence is equal to the dissipation. If we assume that all the energy in modes above 10 is dissipated by the 3000-m isobath, then $D \approx (\Delta x)^{-1} \Sigma_{11}^{\infty} F_n$. We use the knife-edge model with the background stratification and a reasonable tidal velocity to calculate F_n for ridges of depth between 0 and 4700 m. From that we calculate D and $E = \Sigma_1^{\infty} c_n^{-1} F_n$ for each height and compare the results (Fig. 13). For ridges with depths between 200 and 3000 m a power law is found $D \sim E^{0.9}$.

A more sophisticated model is investigated in the appendix, which uses decay time scales to remove energy from the waves, presumably via nonlinear wave–wave interactions. In this model, the high modes propagate slowly and dissipate near the ridge, justifying the

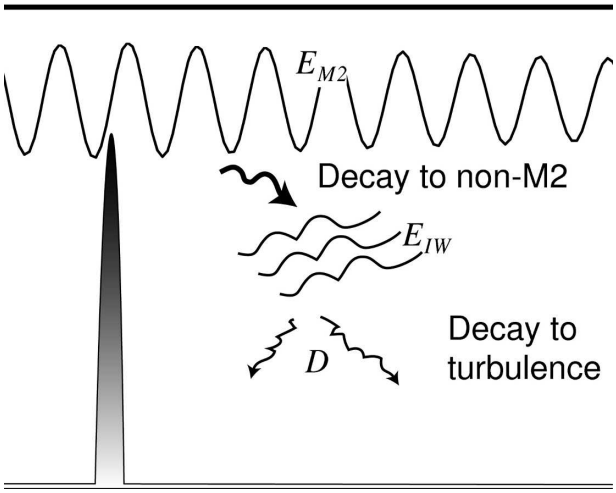

FIG. 12. Schematic of internal tide energy cascade. Energy cascades from the internal tide to the continuum (E_{IW}), after which it cascades to turbulence.

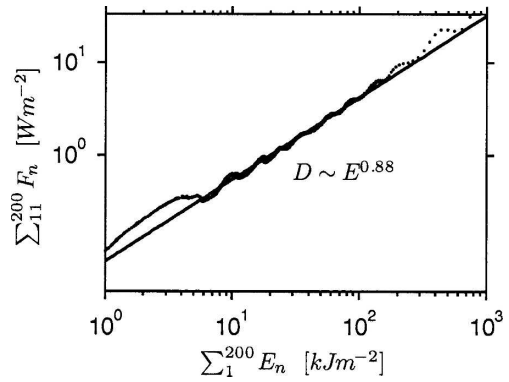

FIG. 13. Comparison of energy flux of modes above 10 to the total energy density. Calculation is for ridge depths between 0 and 4700 m, assuming the same stratification and off-ridge barotropic velocity for all ridges. The fit is made for ridges between 200 and 3000 m deep.

simple mode-truncation model. However, there is also a significant contribution from the energetic low modes that the mode-truncation model ignores. In either case, these simple models indicate that the along-ridge dissipation scales with the M_2 energy density approximately linearly.

6. Along-ridge integration of dissipation

In this section, we make a rough estimate of the integrated dissipation near the ridge. It should be clear from our sparse sampling of 2500 km that this attempt will be imprecise (Fig. 2). We extend the cross-ridge structure (section 4) to the rest of the ridge, scaling it so that the dissipation is consistent with the M_2 energy density, $D \sim E^{1.0}$. Since we did not measure E over most of the ridge, we use the results from the numerical model of MH02.

The MH02 values of E_M, spaced every 3 km, were smoothed in two dimensions with an 18-km boxcar filter to remove granularity in the model. Where the ridge crest was deeper than 3000 m we use the shallowest point for E_M. We normalize these values at KC, x_{KC}, and then multiply by the value of $\mathcal{D}(x_{\mathrm{KC}}) = 1.6\ \mathrm{kW\ m^{-1}}$ derived for KC (Fig. 8):

$$\mathcal{D}(x) = \left[\frac{E_M(x)}{E_M(x_{\mathrm{KC}})}\right]^p \mathcal{D}(x_{\mathrm{KC}}). \tag{7}$$

If we take $p = 1.0$, then integrating along the ridge gives a total of $\int \mathcal{D}\,dx = 3$ GW of dissipation (Fig. 14b, thick line). The highest dissipations are at KC, FFS, and Nihoa Island, where they peak near $\mathcal{D}(x) = 2.5\ \mathrm{kW\ m^{-1}}$ (a little less than 2 times the one-sided dissipation at KC, since this number is now for both the north and south sides of the ridge). If we had scaled by the smaller $\mathcal{D}(x_{\mathrm{KC}}) = 1.4\ \mathrm{kW\ m^{-1}}$ estimated for weaker dissipation shallower than 500 m on the ridge tops, then we would get a dissipation rate of 2.6 GW.

The power law from the scattered data in Fig. 11 was not well constrained. Lowering the power to $p = 0.5$ tends to deemphasize peak internal tide production areas and gives a higher value for the total dissipation of 4.5 GW. Increasing the power to $p = 1.5$ deemphasizes the weak dissipation regions, giving a lower estimate of 2 GW.

These are very rough estimates that we feel are consistent with the sparse data collected along the ridge. The steps we have followed are as follows:

1) Find cross-ridge $[\chi(y/L)]$ and vertical $[\zeta(z/H)]$ structures consistent with the observed data.
2) Construct a two-dimensional section at Kauii Channel that yields a dissipation rate per length of ridge $[\mathcal{D}(x_{KC})]$.
3) Extrapolate the dissipation along ridge assuming that dissipation obeys a simple power law with M_2 tidal energy E, which we estimate from the numerical model of MH02 $[\mathcal{D}(x) \sim E_M(x)^{1\pm0.5}]$.

Each step has large uncertainties and represents gross idealizations. Interpolating to make a two-dimensional section may smooth over irregularities in the dissipation rate. The final step of extending the data along the ridge is quite ambitious given the sparse sampling and scatter of the data that went into the power law upon which it was based. While the spread of estimates here is 2–4.5 GW, there are errors that we are surely underestimating. In light of this, we assign an

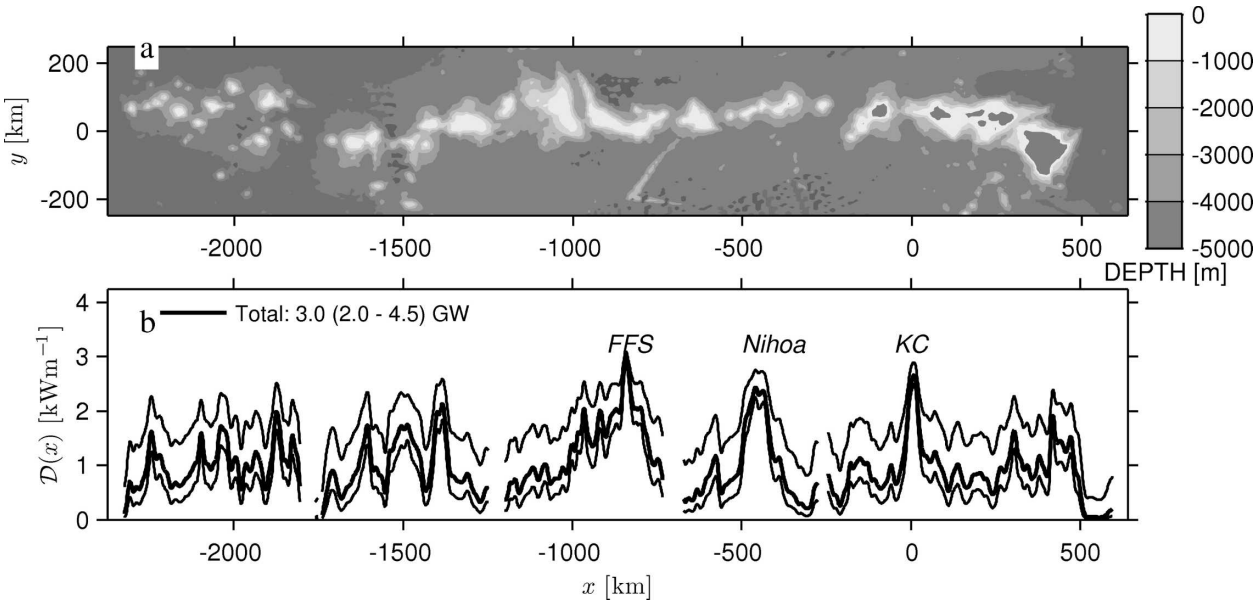

FIG. 14. (a) Topography of the ridge, rotated into along- and cross-ridge direction. (b) Dissipation estimates along the ridge (both sides summed) for $\mathcal{D}(x) \sim E_M(x)^{1\pm0.5}$. The along-ridge data have been smoothed to 25 km for presentation purposes.

error of 50% to our base model to give 3 ± 1.5 GW of dissipation near the ridge.

7. Discussion

a. Comparison with Brazil Basin observations

There are few direct measurements of turbulence dissipation in the deep ocean. The most complete dataset was collected in the Brazil Basin (Polzin et al. 1997). There is weak turbulence in the west side of the basin, where the seafloor is relatively smooth, and strong turbulence in the east, where the topography is relatively rough. The depth dependence of dissipation in the east is quite similar to that observed here (St. Laurent and Nash 2004). The heightened turbulence near the seafloor is identified with internal tides generated at the rough topography of the basin, which decays due to wave–wave interactions and dissipation as they radiate upward (Polzin 2004). A similar internal tide generation mechanism has been suggested by St. Laurent and Garrett (2002) and applied to the global ocean, with an empirical decay scale, that predicts a halo of dissipation with distance from the seafloor (Simmons et al. 2004).

The observations here have a similar depth dependence to those from the Brazil Basin. However, they also have a strong cross-ridge component. Dissipation is very high over the ridge crest and decreases rapidly away from the ridge. This cross-ridge dependence is in addition to, and stronger than, the vertical dependence. We have explained this in terms of the decay of horizontally propagating internal modes rather than as vertically propagating free waves; however, the idea is the same. That this model roughly predicts the dependence of dissipation on the internal tidal energy is encouraging. The fact that we do not find a strong spring–neap cycle near the ridge also indicates that the tide undergoes wave–wave interactions that decouple the dissipation from direct forcing of the tide.

In fact, the similarity of the depth dependence between HOME and the Brazil Basin may be a coincidence. Levine and Boyd (2006) estimate turbulence using the overturning method from data obtained on a mooring located on the north side of KC in 1450 m of water. They found $\varepsilon \approx 2 \times 10^{-8}$ m^2 s^{-3} between 1450 and 1300 m, and $\varepsilon \approx 1.5 \times 10^{-9}$ m^2 s^{-3} at 1150 m. These numbers are in agreement with our dissipation estimates for these depths (Fig. 8). However, Levine and Boyd (2006) show that the near-bottom dissipation in Hawaii has a cubic dependence on the spring–neap cycle of the tide and is also locked to the phase of the internal tide, indicating a direct breaking of the tide. This direct forcing of the near-bottom turbulence is unique from the wave–wave interactions proposed for the depth dependence in the Brazil Basin. Of course, the two effects are not mutually exclusive, and there may be generation and scattering of internal tides along the rough floor near Hawaii that produce vertically propagating waves in addition to the direct breaking.

This suggests two different models for the structure of dissipation depending on whether the dominant to-

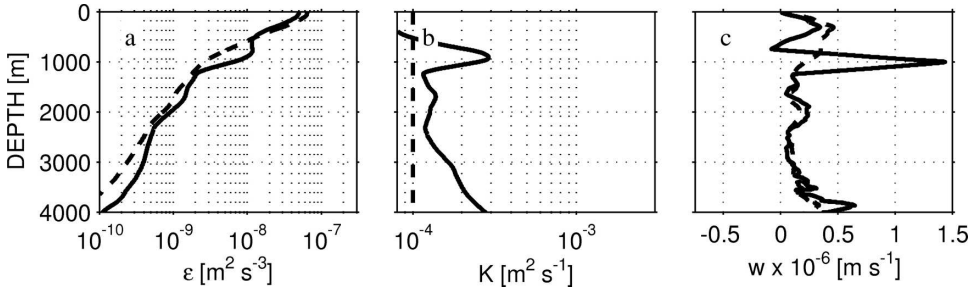

FIG. 15. The 60-km cross-ridge average profiles inferred from structure of turbulence at KC (Fig. 8). (a) Mean dissipation. Dashed line is for $\varepsilon = 5 \times 10^{-4} N^2$, the canonical value if $K = 10^{-4}$ m^2 s^{-1}. (b) Mean diffusivity; dashed line is canonical value. (c) Vertical velocity that can be supported by the inferred mixing; dashed line is for canonical value.

pography is super- or subcritical with respect to the M_2 tide. If subcritical, the decay of turbulence is generally in the vertical, as suggested by Polzin (2004) and employed by Simmons et al. (2004). If supercritical, we suggest that the dominant decay is horizontal, which will require somewhat different parameterizations. We have not constrained at what depths the strengthened turbulence will act. However, the relatively constant K_ρ profiles above the bottom indicate that $\varepsilon(z) \sim N^2$.

b. Importance to mixing

The average of our structure $K(y, z)$ in y shows that the average diffusivity near KC is higher than the canonical value of $K_\rho \approx 10^{-4}$ m^2 s^{-1} given by Munk (1966), but only by a factor of 2 at most depths. There is a notable bulge between 700 and 1000 m, where the diffusivity is $K_\rho \approx 3 \times 10^{-4}$ m^2 s^{-1}, caused by heightened dissipation over the ridge crest. Deeper, the diffusivity rises because of the imposed near-bottom increase from 4000 to 2500 m, with some enhancement due to the ridge shoaling.

The average profiles can be put into the context of a local advective–diffusive balance in the spirit of Munk and Wunsch (1998). Convergence or divergence of buoyancy flux can be offset by upwelling (or downwelling). To good approximation,

$$w = 0.2\langle N\rangle^{-2} \frac{\partial}{\partial z}\langle \varepsilon \rangle, \tag{8}$$

where brackets represent averages over a basin, and w is the average upwelling through any isopycnal (note that for a nonrectangular basin, the order of the operations is relevant and should be carried out as described here). The vertical velocity implied by this calculation is not significantly larger than that implied by $K_\rho = 10^{-4}$ m^2 s^{-1} except near the bulge over the ridge, where there is enhanced upwelling deeper than 850 m and downwelling above 850 m (Fig. 15c). We can estimate the horizontal velocity that this convergence implies as $u = w\Delta x/\Delta z \approx 10^{-3}$m s^{-1}, so the direct effect on the circulation near the ridge is negligible.

The calculation above is just for Kauai Channel. The average diffusivity for the whole ridge can be estimated from the dissipation estimates made above. The result is surprisingly depth invariant (Fig. 16); while shallow parts of the ridge have more dissipation, more of the ridge is deep. In total, the average diffusivity within 60

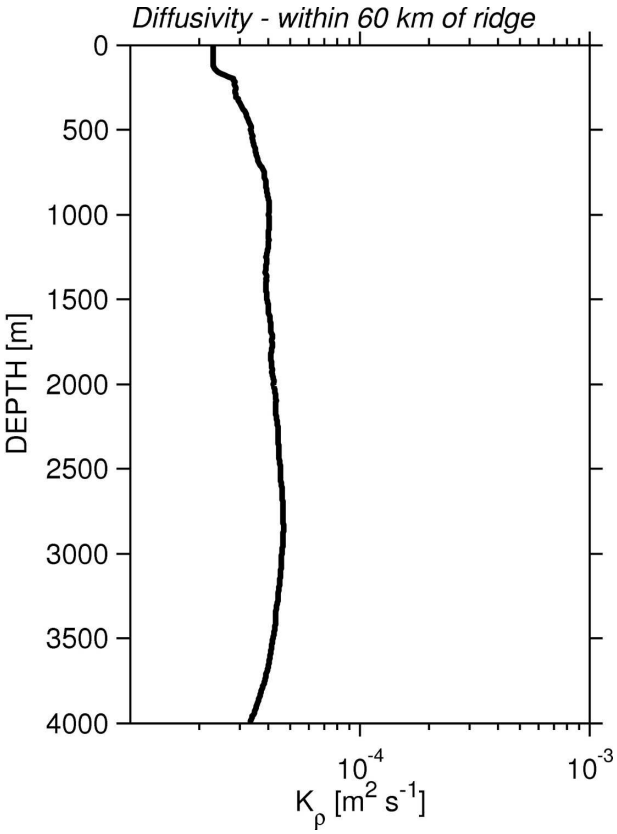

FIG. 16. Profile of diffusivity for the whole length of the ridge, averaged within 60 km.

km is not strong enough to bring the mean value to that required by Munk (1966). Note that this profile only represents the average of what we have extrapolated in this paper. Mixing due to the rest of the energy removed from the tide will be higher than in this profile; we do not have an estimate of where.

If we consider the mixing from the point of view of finding the 1 TW of energy needed for mixing deeper than 1000 m (Munk and Wunsch 1998), dissipation like that found near Hawaii is not very efficient (Lee et al. 2006). Of the 1.6 kW m^{-1} of dissipation in Fig. 8, only 0.2 kW m^{-1}, or %12, is dissipated below 1000 m. If the rest of the 18 GW of energy lost from the barotropic tide dissipates in a similar fashion, Hawaii will only supply about 2 GW of energy to the abyssal ocean, and 500 other similar sources of dissipation will need to be found to drive abyssal upwelling. Egbert and Ray (2000) find approximately 1 TW of energy loss in the abyssal ocean; however, again, if this dissipates with the same vertical structure as Hawaii, only 0.1 TW will be available for mixing deeper than 1000 m.

c. *Radiation efficiency*

A number of simple models do a reasonable job of estimating the energy removed from the barotropic tide at the important internal tide generation sites. For instance, the idealized models presented by St. Laurent et al. (2003) and the global internal tide generation model presented by Simmons et al. (2004) both predict near 20 GW of energy removed from the M_2 internal tide near Hawaii. These models are linear, or almost linear, whereas the actual generation is highly nonlinear. For these models to be complete, we must know how much energy is radiated away as low-mode internal waves versus dissipated locally.

The results here indicate that the radiation efficiency at KC is quite high. Approximately 20 kW m^{-1} of energy is radiated from stations at KC (Fig. 10) (Lee et al. 2006), whereas we estimate 1.6 kW m^{-1} dissipated locally (Fig. 8). Therefore, approximately 90% of the energy lost from the barotropic tide is radiated away at this location. This percentage applies for the whole length of the ridge if we use the scaling $D \approx E^1$. If 18 ± 6 GW of energy is lost from the barotropic tide (Egbert and Ray 2000) and 3 ± 1.5 GW is dissipated via turbulence within 60 km of the ridge, then 8%–25% of the tidal energy is dissipated near the ridge. The remaining 92%–75% is not accounted for here and presumably radiates away as internal waves.

Of course, this energy budget ignores other potential sources of turbulence dissipation beyond the M_2 tide. There is also near-inertial and submesoscale energy, though presumably neither of these would elevate turbulence or mixing above the background oceanic value. (Zaron and Egbert 2006) estimate 22 GW lost from the six most important tidal constituents, so there is potentially another 4 GW of tidal energy in the system, increasing the radiation efficiency even more. We have no way of addressing these complications in the present dataset.

There are not many direct measurements of energy radiation from internal tide generation sites like this. Althaus et al. (2003) estimated that near Mendocino Escarpment, a long isolated ridge that is also perpendicular to the tidal forcing, 99% of the energy radiates away as internal tides. Klymak and Gregg (2004) estimated that in Knight Inlet, a fjord with a sharp sill, 66% of the energy radiates away as tidal waves, the rest being dissipated by the violent nonlinear waves or vortices shed by the constriction. That the majority of the energy radiates away from the generation sites leaves an open question as to where it ultimately dissipates. This question is the subject of ongoing research. Recently, Nash et al. (2004) suggested that offshore tides may be focused and caused to dissipate at continental slopes. Another possible sink is enhanced subharmonic instabilities at latitudes where $M_2 = f$ (MKW).

8. Conclusions

An integrated analysis of observations from four unique instruments made in two separate experiments highlights the characteristics of the dissipation near the Hawaiian Ridge. The analysis indicates

- an increase of diffusivity near the seafloor;
- very high diffusivity over the ridge crests, $K > 10^{-3}$ $m^2 s^{-1}$ over the ridge saddles, decreasing rapidly over the flanks to $K \approx 10^{-4}$ $m^2 s^{-1}$ over 10 km;
- a gradual drop in the next 30 km to $K \approx 10^{-5}$ $m^2 s^{-1}$;
- a factor-of-2 difference in diffusivity between neap and spring;
- a dependence of diffusivity on the M_2 energy density, such that the vertically integrated dissipation $D \sim E^{1\pm0.5}$; and
- approximately 3 ± 1.5 GW of energy dissipated near the ridge.

The energy budget presented in the introduction of 18 ± 6 GW lost from the barotropic tide (Egbert and Ray 2000) going into either internal wave or dissipation is not closed by this analysis. If the estimates of 10 GW radiating away from the ridge (in M_2) are credible, then there is still between 7 and 4 GW unaccounted for. The extrapolations made in this paper are necessarily quite rough; it is very conceivable that there are hot spots of turbulence not accounted for by our observations. The

work of Finnigan et al. (2002) suggests one possible site, 50 km north of Kauai Channel. There is also evidence from Mendocino Escarpment that there is considerable dissipation at the first surface bounce of internal tide beams (Althaus et al. 2003). Our sampling made an effort to examine this, but the results were inconclusive (Carter et al. 2006). It is also possible that the MH02 model underpredicts when it estimates 10 GW radiating away as internal tides.

Acknowledgments. We thank the captains and crews of the R/V *Wecoma* and R/V *Revelle*. John Dunlap, Robert Drever, Art Bartlett, Mike Neeley-Brown, Ray Kreth, Greig Thompson, Jack Miller, Stephen Bayer, Earl Krause, David Winkel, Eric Boget, Dicky Allison, Alana Althaus, and John Mickett all made collecting these datasets possible. Mark Merrifield kindly provided model output. Alexander Perlin helped with early processing and data collection. We had valuable discussions with Gary Egbert, Doug Luther, and Jennifer MacKinnon. Rob Pinkel, Dan Rudnick, and Doug Luther organized HOME and hosted productive workshops where much of this material was discussed and improved by input from all the investigators in the HOME group. Two anonymous reviewers had excellent comments that helped this manuscript substantially. This work was funded by the National Science Foundation (Grants 9819537, 9819531, and 9819522).

APPENDIX

Scaling the Dissipation to the Internal Tide Generation

We observed that dissipation is proportional to the baroclinic M_2 tidal energy ($E^{1.2\pm0.3}$) at the 3000-m isobath. Dissipation has been found to be quadratically proportional to the energy level of the broadband wave field, so the weak dependence of the turbulence dissipation on the M_2 forcing is intriguing. A possible explanation can be found by considering the situation where there is a localized source of the internal tide at $y = 0$. If we know the energy generated in each vertical mode $E_n^{(0)}$ at the source, and we further know a decay time scale for each mode τ_n, then the wave energy and the wave flux are given by

$$E(y) = \sum_n E_n = \sum_n E_n^0 e^{-\frac{y}{c_n\tau_n}} \tag{A1}$$

and

$$F(y) = \sum_n F_n = \sum_n c_n E_n^0 e^{-\frac{y}{c_n\tau_n}}, \tag{A2}$$

where c_n is the group speed of mode n, and the summation is over all vertical modes. If we further assume that the energy level is in steady state everywhere, then the rate at which energy is removed from the internal tide is equal to the horizontal divergence of the flux, which, in one dimension, is given by

$$\nabla F = \sum_n E_n^0 \frac{\partial}{\partial y}\left(\frac{y}{\tau_n}\right) e^{-\frac{y}{c_n\tau_n}}. \tag{A3}$$

We have left τ_n to be differentiated in case it changes with y. If τ_n is a constant for each n, then we have

$$\nabla F = \sum_n \frac{E_n^0}{\tau_n} e^{-\frac{y}{c_n\tau_n}}. \tag{A4}$$

For the decay time scale τ_n, we use the weak interaction theory developed by Pomphrey et al. (1980). This theory predicts how long it will take a wave at M_2 frequency to lose its energy by interaction with a background internal wave field as described by the canonical open-ocean spectrum (Munk 1981). This time scale approximately scales with mode number as $\tau_n = 10^7 n^{-3/2}$ s, so that the first mode has a decay time scale of 115 days.

To estimate the energy generated in each mode E_n^0 we use a simple knife-edge model (Llewellyn Smith and Young 2003; St. Laurent et al. 2003). Working in a WKB-stretched coordinate system,

$$Z = \frac{\pi}{h}\int_0^z N(z')/\langle N(z)\rangle \, dz', \tag{A5}$$

the height of the ridge from the seafloor is b in real coordinates and B in stretched coordinates; then the production of internal wave energy is [Llewellyn Smith and Young 2003, their Eq. (5.12)]

$$F = \frac{\pi}{4}\rho_0 U^2 \sqrt{1 - \frac{f^2}{\omega^2}} N(b) b^2 M(B/\pi), \tag{A6}$$

where $U_0 = 0.03$ m s^{-1}, f and ω are the Coriolis and tidal frequencies, and $M(B/\pi)$ is given by

$$M(B/\pi) = \frac{4}{\pi B^2}\int_0^B Z\sqrt{\frac{1-\cos Z}{\cos Z - \cos B}}\, dZ. \tag{A7}$$

As pointed out by Llewellyn Smith and Young (2003), this is best evaluated numerically with the substitution $t = \tan(Z/2)$, which makes the integral

$$M(B/\pi) = \frac{16\sqrt{1+\tau^2}}{\pi B^2}\int_0^\tau \frac{t\tan^{-1}t}{\sqrt{\tau^2 - t^2}}\frac{dt}{1+t^2}. \tag{A8}$$

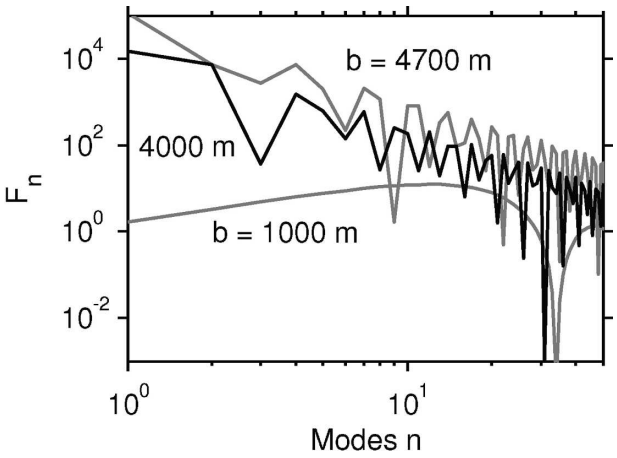

FIG. A1. Distribution of wave-flux energy into vertical modes for the knife-edge model at three different ridge heights (b) in 5000 m of water.

The projection of F onto vertical modes is also derived as

$$F_n(B/\pi) = Fk^{-1}PP_k^2/\sum_{k=1}^{\infty} k^{-1}PP_k^2, \qquad \text{(A9)}$$

where $PP_k = P_{n-1}(\cos B) - P_n(\cos B)$, and P_k is the kth Legendre polynomial. The results of this calculation for our stratification $N(z)$ and a water depth of 5000 m is shown in Fig. A1 for three different ridge heights.

Putting these components together, we have a rough model for the cascade of energy in a wave field generated by a knife edge (Fig. 12). The internal tide is generated with a flux in each mode E_n. The internal tidal waves interact nonlinearly with the continuum field (and perhaps with each other) to put more energy into the continuum wave field (E_{IW}).

The power-law dependence of the dissipation becomes apparent when depth-integrated flux divergence (which we are equating with dissipation) is compared with the depth-integrated energy density (Fig. A2). The dissipation follows a rough power law, with some curvature at the highest and lowest energy densities, corresponding to shallow and deep ridges. Fitting the modeled curves to a power law between the results corresponding to ridges 2500 and 200 m deep gives values of the exponent between 0.9 near the ridge and 0.8 at 50-km distance.

A last point is that the model assumes that the loss of energy from the M_2 internal tide goes directly to local dissipation. There is an implicit assumption that the M_2 internal tidal energy is fed into the continuum wave field that subsequently dissipates the energy (as pictured in Fig. 12). There is evidence that the continuum internal wave field drives the dissipation consistent with the open-ocean scaling of $D \approx E_{\mathrm{IW}}^2$ (Lee et al. 2006). This implies that the internal wave field will have a weak variation along the ridge as z_r changes: $E_{\mathrm{IW}} \approx E_{M_2}^{1/2}$.

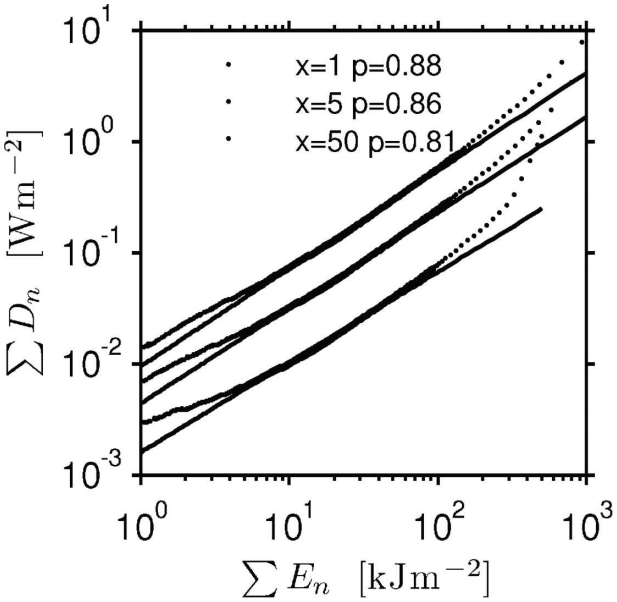

FIG. A2. Depth-integrated dissipation as a function of depth-integrated energy density. Power law is fit between b = 2500 m and b = 4800 m.

REFERENCES

Althaus, A. M., E. Kunze, and T. B. Sanford, 2003: Internal tide radiation from Mendocino Escarpment. *J. Phys. Oceanogr.,* **33,** 1510–1527.

Carter, G. S., and M. C. Gregg, 2002: Intense, variable mixing near the head of Monterey Submarine Canyon. *J. Phys. Oceanogr.,* **32,** 31–45.

——, ——, and M. A. Merrifield, 2006: Flow and mixing around a small seamount on Kaena Ridge, Hawaii. *J. Phys. Oceanogr.,* **36,** 1036–1052.

Egbert, G. D., and R. D. Ray, 2000: Significant dissipation of tidal energy in the deep ocean inferred from satellite altimeter data. *Nature,* **405,** 775–778.

Finnigan, T., D. Luther, and R. Lukas, 2002: Observations of enhanced diapycnal mixing near the Hawaiian Ridge. *J. Phys. Oceanogr.,* **32,** 2988–3002.

Ganachaud, A., and C. Wunsch, 2000: Improved estimates of global ocean circulation, heat transport and mixing from hydrographic data. *Nature,* **408,** 453–457.

Gregg, M. C., 1989: Scaling turbulent dissipation in the thermocline. *J. Geophys. Res.,* **94,** 9686–9698.

Henyey, F. S., J. Wright, and S. M. Flatté, 1986: Energy and action flow through the internal wave field. *J. Geophys. Res.,* **91,** 8487–8495.

Klymak, J. M., and M. C. Gregg, 2004: Tidally generated turbulence over the Knight Inlet sill. *J. Phys. Oceanogr.,* **34,** 1135–1151.

Kunze, E., and J. M. Toole, 1997: Tidally driven vorticity, diurnal

shear, and turbulence atop Fieberling Seamount. *J. Phys. Oceanogr.,* **27,** 2663–2693.

Ledwell, J., A. Watson, and C. Law, 1993: Evidence for slow mixing across the pycnocline from an open-ocean tracer-release experiment. *Nature,* **364,** 701–703.

Lee, C. M., E. Kunze, T. B. Sanford, J. D. Nash, M. A. Merrifield, and P. E. Holloway, 2006: Internal tides and turbulence along the 3000-m isobath of the Hawaiian Ridge. *J. Phys. Oceanogr.,* **36,** 1165–1183.

Levine, E. R., and R. G. Lueck, 1999: Turbulence measurements with an autonomous underwater vehicle. *J. Atmos. Oceanic Technol.,* **16,** 1533–1544.

Levine, M. D., and T. J. Boyd, 2006: Tidally forced internal waves and overturns observed on a slope: Results from HOME. *J. Phys. Oceanogr.,* **36,** 1184–1201.

Llewellyn Smith, S. G., and W. R. Young, 2003: Tidal conversion at a very steep ridge. *J. Fluid Mech.,* **495,** 175–191.

Marsden, R. F., 1999: A proposal for a neutral regression. *J. Atmos. Oceanic Technol.,* **16,** 876–883.

Merrifield, M. A., and P. E. Holloway, 2002: Model estimate of M2 internal tide energetics at the Hawaiian Ridge. *J. Geophys. Res.,* **107,** 3179, doi:10.1029/2001JC000996.

Moum, J. N., 1996: Energy-containing scales of turbulence in the ocean thermocline. *J. Geophys. Res.,* **101,** 14 095–14 109.

——, M. C. Gregg, R. C. Lien, and M. Carr, 1995: Comparison of turbulence kinetic energy dissipation rate estimates from two ocean microstructure profilers. *J. Atmos. Oceanic Technol.,* **12,** 346–366.

——, D. R. Caldwell, J. D. Nash, and G. D. Gunderson, 2002: Observations of boundary mixing over the continental slope. *J. Phys. Oceanogr.,* **32,** 2113–2130.

Munk, W. H., 1966: Abyssal recipes. *Deep-Sea Res.,* **13,** 707–730.

——, 1981: Internal waves and small-scale processes. *Evolution of Physical Oceanography,* B. A. Warren and C. Wunsch, Eds., MIT Press, 264–291.

——, and C. Wunsch, 1998: Abyssal recipes II: Energetics of tidal and wind mixing. *Deep-Sea Res.,* **45,** 1977–2010.

Nash, J. D., E. Kunze, J. M. Toole, and R. W. Schmitt, 2004: Internal tide reflection and turbulent mixing on the continental slope. *J. Phys. Oceanogr.,* **34,** 1117–1134.

——, M. H. Alford, and E. Kunze, 2005: Estimating internal wave energy fluxes in the ocean. *J. Atmos. Oceanic Technol.,* **22,** 1551–1570.

Olbers, D. J., 1983: Models of the oceanic internal wave field. *Rev. Geophys Space Phys.,* **21,** 1567–1606.

Osborn, T. R., 1980: Estimates of the local rate of vertical diffusion from dissipation measurements. *J. Phys. Oceanogr.,* **10,** 83–89.

Polzin, K., 2004: Idealized solutions for the energy balance of the finescale internal wave field. *J. Phys. Oceanogr.,* **34,** 231–246.

——, N. S. Oakey, J. M. Toole, and R. W. Schmitt, 1996: Fine structure and microstructure characteristics across the northwest Atlantic subtropical front. *J. Geophys. Res.,* **101,** 14 111–14 121.

——, J. Toole, J. Ledwell, and R. Schmitt, 1997: Spatial variability of turbulent mixing in the abyssal ocean. *Science,* **276,** 93–96.

Pomphrey, N., J. D. Meiss, and K. M. Watson, 1980: Description of non-linear inernal wave interactions using Langevin methods. *J. Geophys. Res.,* **85,** 1085–1094.

Ray, R., and D. Cartwright, 2001: Estimates of internal tide energy fluxes from TOPEX/Poseidon altimetry: Central North Pacific. *Geophys. Res. Lett.,* **28,** 1259–1262.

Rudnick, D. L., and Coauthors, 2003: From tides to mixing along the Hawaiian Ridge. *Science,* **301,** 355–357.

Sanford, T. B., R. G. Drever, and J. H. Dunlap, 1985: An acoustic Doppler and electromagnetic velocity profiler. *J. Atmos. Oceanic Technol.,* **2,** 1254–1257.

Simmons, H. L., R. W. Hallberg, and B. K. Arbic, 2004: Internal wave generation in a global baroclinic tide model. *Deep Sea Res. II,* **51,** doi:10.1016/j.dsr2.2004.09.015.

Stigebrandt, A., 1980: Some aspects of tidal interaction with fjord constrictions. *Estuar. Coast. Mar. Sci.,* **11,** 151–166.

St. Laurent, L., and C. Garrett, 2002: The role of internal tides in mixing the deep ocean. *J. Phys. Oceanogr.,* **32,** 2882–2899.

——, and J. D. Nash, 2004: On the fraction of internal tide energy dissipated near topography. *Near-Boundary Processes and Their Parameterization: Proc. 'Aha Huliko'a Hawaiian Winter Workshop,* Honolulu, HI, University of Hawaii at Manoa, 45–58.

——, J. M. Toole, and R. W. Schmitt, 2001: Buoyancy forcing by turbulence above rough topography in the abyssal Brazil Basin. *J. Phys. Oceanogr.,* **31,** 3476–3495.

——, S. Stringer, C. Garrett, and D. Perrault-Joncas, 2003: The generation of internal tides at abrupt topography. *Deep Sea Res. I,* **50,** doi:10.1016/S0967-0637(03)00096-7.

Wesson, J. C., and M. C. Gregg, 1994: Mixing at Camarinal Sill in the Strait of Gibraltar. *J. Geophys. Res.,* **99,** 9847–9878.

Zaron, E. D., and G. D. Egbert, 2006: Estimating open-ocean barotropic tidal dissipation: The Hawaiian Ridge. *J. Phys. Oceanogr.,* **36,** 1019–1035.